SURFACE AND INTERFACE PHONON POLARITON CHARACTERISTICS OF WURTZITE ZnO-BASED SEMICONDUCTOR BY INFRARED ATTENUATED TOTAL REFLECTION SPECTROSCOPY

LEE SAI CHEONG

UNIVERSITI SAINS MALAYSIA

2011

SURFACE AND INTERFACE PHONON POLARITON

CHARACTERISTICS OF WURTZITE ZnO-BASED SEMICONDUCTOR BY

INFRARED ATTENUATED TOTAL REFLECTION SPECTROSCOPY

by

LEE SAI CHEONG

Thesis submitted in fulfillment of the

requirements for the degree

of Master of Science

September 2011

ACKNOWLEDGEMENTS

TABLE OF CONTENTS

LIST OF TABLES

LIST OF FIGURES

LIST OF SYMBOLS

ε_∞	High frequency dielectric constant
$\parallel$	Parallel
$\perp$	Perpendicular
c	Velocity of light in a vacuum (3×10^8 ms^{-1})
c_{axis}	Optical axis
$\varepsilon_{xx\,(yy,\,zz)}$	Dielectric function component in x- (y-, z-) direction
$\varepsilon_{\perp\,(\parallel)}$	Dielectric function component in a direction perpendicular (parallel) to the c_{axis}
$D_{x\,(y,\,z)}$	Electric displacement field component along the x- (y-, z-) direction
$E_{x\,(y,\,z)}$	Electric field components along the x- (y-, z-) direction
$H_{x\,(y,\,z)}$	Auxiliary magnetic field component along the x- (y-, z-) direction
N	Total number of layers
l	Specific layer in a multilayer system
m	Interface between layer l and layer $l+1$
d	Finite thickness of a thin film
k_p	In-plane wavevector component of evanescent wave generated by ATR crystal

k_{sub}	Wavevector of the substrate light line
k_{vac}	Wavevector of the vacuum light line
k_x	Wavevector of SP along the x-direction
n	Refractive index
n_p	Refractive index of the ATR crystal
q_x	Wavevector component of the incident light in x-direction
α	Field decay constants along the normal of the interface
γ_{LO}	Longitudinal optical phonon damping constant
γ_{TO}	Transverse optical phonon damping constant
γ_p	Plasma damping constant
θ	Angle of incidence in the medium of incidence
θ_c	Critical angle
ω	Angular frequency
ω_{LO}	Longitudinal optical phonon frequency
ω_{TO}	Transverse optical phonon frequency
ω_p	Plasma frequency
$r_{s\,(p)}$	s- (p-) polarized IR reflection coefficient
$R_{s\,(p)}$	s- (p-) polarized IR reflectivity

LIST OF ABREVIATIONS

AlGaN	Aluminum gallium nitride
AlN	Aluminum nitride
ATR	Attenuated total reflection
BPP	Bulk phonon polariton
CaF_2	Calcium fluoride
CdF_2	Cadmium fluoride
CuSCN	Copper (I) thiocyanate
EM	Electromagnetic
FTIR	Fourier Transform infrared
GaAs	Gallium arsenide
GaN	Gallium nitride
GaP	Gallium phosphide
InN	Indium nitride
IPP	Interface phonon polariton
IR	Infrared
IRE	Internal reflection element
KRS-5	Thallium iodide bromide
$KTaO_3$	Potassium tantalate
LO	Longitudinal optical
RF	Radio frequency
SiC	Silicon carbide
SP	Surface polariton
SPP	Surface phonon polariton

SrTiO$_3$	Strontium titanate
TE	Transverse electric
TM	Transverse magnetic
TO	Transverse optical
ZnO	Zinc oxide
ZnTe	Zinc telluride

CIRI-CIRI POLARITON FONON PERMUKAAN DAN ANTARAMUKA BAGI SEMIKONDUKTOR BERASASKAN WURTZIT ZnO MENGGUNAKAN SPEKTROSKOPI PANTULAN PENUH DIKECILKAN INFRAMERAH

ABSTRAK

Kajian ciri-ciri polariton fonon permukaan (SPP) bagi semikonduktor berasaskan wurtzit zink oksida (ZnO) telah dilaporkan. Tumpuan diberikan kepada kajian mod polariton fonon permukaan dan fonon antara muka (IPP) dalam sistem heterostruktur ZnO. Sebagai perbandingan, mod SPP dalam kristal ZnO pukal juga telah dikaji. Usaha awal bermula dengan terbitan hubungan penyebaran permukaan polariton (SP) untuk sistem berbilang lapisan berasaskan wurtzit. Perumusan yang diperoleh telah digunakan untuk mengkaji ciri-ciri penyebaran bagi mod SPP dan IPP dalam kristal ZnO pukal, filem nipis ZnO di atas substrat 6H-SiC, dan heterostruktur ZnO/GaN di atas substrat 6H-SiC. Untuk mengesahkan keputusan teori, pengukuran pantulan penuh dikecilkan (ATR) inframerah (IR) terkutub-p telah dijalankan. Keputusan yang diperoleh bersetuju dengan spektrum teori yang disimulasi oleh teknik optik berbilang lapisan piawai. Melalui perbandingan data eksperimen dan lengkung penyebaran SP, asal-usul bagi mod yang diperhatikan telah disahkan.

Sepanjang kajian ini, satu perumusan baru bagi hubungan penyebaran SP telah berjaya diterbitkan melalui penyelesaian persamaan elektromagnet (EM) Maxwell secara langsung berdasarkan teknik manipulasi algebra. Secara umum, bilangan cabang SP sangat bergantung kepada penyetempatan di antara muka.

Sementara itu, ketebalan lapisan epitaksi mempunyai pengaruh yang penting ke atas sifat-sifat penyebaran mod SPP dan IPP. Selain daripada itu, ia telah ditunjukkan bahawa frekuensi mod kebocoran dapat diramalkan dengan mengambil kira peredaman substrat dalam pengiraan berangka bagi lengkung penyebaran SP.

SURFACE AND INTERFACE PHONON POLARITON CHARACTERISTICS OF WURTZITE ZnO-BASED SEMICONDUCTOR BY INFRARED ATTENUATED TOTAL REFLECTION SPECTROSCOPY

ABSTRACT

Studies of surface phonon polariton (SPP) characteristics of wurtzite zinc oxide (ZnO) based semiconductors were reported. Attention was paid on the investigations of the SPP and also the interface phonon polariton (IPP) modes in the ZnO heterostructure systems. For comparison, the SPP mode in the bulk ZnO crystal was also investigated. The early effort started with the derivation of the surface polariton (SP) dispersion relations for wurtzite based multilayer systems. The obtained formulations were applied to investigate the dispersion properties of the SPP and IPP modes in the bulk ZnO crystal, ZnO thin film on 6H-SiC substrate, and ZnO/GaN heterostructure on 6H-SiC substrate. To verify the theoretical results, *p*-polarized infrared (IR) attenuated total reflection (ATR) measurements were carried out. The results were in good agreement with the theoretical spectra simulated by the standard multilayer optics technique. Through comparison of the experimental data and the SP dispersion curves, the origins of the observed modes were verified.

Throughout these studies, a new formulation of the SP dispersion relation was successfully developed via solving Maxwell's electromagnetic (EM) equations directly based on algebraic manipulation technique. In general, the number of SP branches strongly depends on the localizations at the interfaces. Meanwhile, the thicknesses of epitaxial layers have an important influence on the dispersion properties of the SPP and IPP modes. Apart from that, it was demonstrated that the

frequencies of the leaky modes can be predicted by taking into account the damping

of the substrate in the numerical calculations of SP dispersion curves.

CHAPTER 1

INTRODUCTION

1.1 Motivation

Zinc oxide (ZnO) belongs to the II-VI group of the periodic table and crystallizes preferentially in the hexagonal wurtzite structure with the lattice parameters $a = 0.3249$ nm and $c = 0.5206$ nm (Jagadish and Pearton, 2006). ZnO is one of the most studied and versatile metal oxide semiconductors in the scientific research community. The strong research interest in ZnO semiconductor is owing to its unique characteristics, which can be utilized to develop various applications (Tang et al., 1998; Matsubara et al., 2003; Fortunato et al., 2005; Tsukazaki et al., 2005; Wang, 2007; Carotta et al., 2009; Kumar et al., 2009).

In recent years, much research devoted to ZnO semiconductor has been directed towards the understanding of its optical and electronic properties. With a wide band gap energy similar to gallium nitride (GaN), i.e., 3.37 eV at 300 K, ZnO is considered as an alternative material to GaN for the design of optoelectronic devices operated in the blue to ultraviolet spectral ranges (Klingshirn, 2007; Wang, 2007). However, ZnO has several advantages in comparison to GaN. The most remarkable advantage of ZnO is that it has a largest exciton binding energy among the III-V and II-VI semiconductors, i.e., 60 meV at 300 K. This properties make ZnO holds promise for highly efficient exciton-based lasing at temperatures even exceeding room temperature (Özgür et al., 2005; Janotti and Van De Walle, 2009). It is also more radiation resistant than GaN and has a higher saturation drift velocity, which offers opportunities for fast electronic applications under extreme environmental

conditions (Klingshirn, 2007). Apart from that, ZnO-based devices have a lower cost of fabrication as compared to the III-nitrides based devices due to the availability of fairly high-quality bulk ZnO single crystal and simpler crystal-growth technology (Özgür et al., 2005).

Semiconductor heterostructure is a structure built up with at least two different semiconductor materials in junction contact (Lamberti, 2008). Integration of ZnO with other materials into heterostructure is one of the key steps to realize ZnO-based device applications (Seo et al., 2002; Kaminska et al., 2004; Alivov et al., 2005; Hwang et al., 2005; Oh et al., 2005; Tena-Zaera et al., 2005; Cagin et al., 2007; Zheng et al., 2008). For examples, a high efficiency photodiode has been successfully fabricated based on a n-ZnO/p-SiC heterostructure (Alivov et al., 2005). An inorganic extreme thin absorber-solar cell has been fabricated based on a ZnO/CdTe/CuSCN heterostructure (Tena-Zaera et al., 2005). Capacitance-voltage characteristics of ZnO/GaN heterostructure suggested that ZnO/GaN heterostructure is a good candidate for application of heterojunction transistor (Oh et al., 2005).

To explore new applications possibility as well as to improve the performance of ZnO-based optoelectronic devices, considerable efforts have been paid to the investigation of the electronic and optical properties in ZnO-based semiconductor heterostructures, especially the ZnO/GaN heterostructure that exhibits a superior electroluminescent characteristic (Kaminska et al., 2002; Yu et al., 2003; Sasa et al., 2007; Titkov et al., 2007; Alivov et al., 2008; Shigehiko et al., 2008; Hwang et al., 2009; Li et al., 2010; Lu et al., 2010; Novodvorskii et al., 2011). Despite of extensive growth and characterization studies of ZnO-based semiconductor heterostructure system, the investigation of its surface and interface

phonon polariton characteristics is still scant and the topic has not received sufficient attention.

It should be noted here that the understanding of the surface and interface phenomena is very important in the fabrication of multi-junction semiconductor device. In a semiconductor multilayer system, properties of the surface and interfaces tend to dominate over the bulk properties of each layer. The existence of the interfaces in semiconductor heterostructure yields dramatically changes of many fundamental properties such as the electron transport and optical phonon properties (Lassnig and Zawadzki, 1984; Chen et al., 1990; Kim and Stroscio, 1990; Wendler et al., 1990; Hsu and Walukiewicz, 1998; Kisin et al., 1998; Zhang et al., 2001; Ohgaki, 2009). While, knowledge on the surface phonon polariton (SPP) and interface phonon polariton (IPP) modes is crucial for understanding the behavior of the coupling effect between the photon and the optical phonons at the heterostructure interfaces (Ng et al., 2007a; 2008b; Zhang, 2008; Zhang and Shi, 2009). From the application point of view, generation and control of the SPP and IPP modes are essential in the novel design of some useful applications. For instances, near field surface enhanced spectroscopy, high density optical data storage device, thermo-photovoltaic energy conversion system, reflection type, and antenna sensors have been developed based on resonant excitation of the SPP mode (Ocelic and Hillenbrand, 2004; Huber et al., 2005; Laroche et al., 2006; Balin et al., 2009; Rousseau et al., 2009; Kim and Cheng, 2010a; Neubrech et al., 2010).

Considering the importance of fundamental properties and also the application potential of the SPP and IPP modes in ZnO-based semiconductor structures, in-depth experimental and theoretical studies of the SPP and IPP characteristics of bulk ZnO crystal, ZnO thin film on 6H-SiC substrate, and

ZnO/GaN heterostructure on 6H-SiC substrate will be carried out. Meanwhile, the optical phonon modes of these materials will also be investigated for the reason that the optical phonon modes are the fundamental parameters for the theoretical studies of the SPP and IPP modes. Through these studies, a better understanding of the SPP and IPP behaviors in wurtzite ZnO-based semiconductor structures can be obtained.

1.2 Objectives and scope of work

The primary objective of this dissertation is to investigate the SPP and IPP characteristics of wurtzite ZnO-based semiconductor structures. The scope of study covers both the theoretical approach and experimental works.

The initial efforts are mainly focused on the theoretical works. These include the simulation of the surface polariton (SP) dispersion curves based on the formulation derived from Maxwell's electromagnetic (EM) equations, the determination of the conditions for the existence of SP branches, and the identification of the origin of each SP branch.

The goal of the latter efforts is to verify the theoretical results with relevant experimental data. The efforts include the determination of the optical parameters and epitaxial layers thicknesses of the samples by the polarized infrared (IR) reflectance measurements, the verification of the observed features in the p-polarized IR attenuated total reflection (ATR) experiments by comparing experimental data with simulations, and the extraction of the information about the SPP and IPP modes from the ATR spectra with the aid of the SP dispersion curves.

1.3 Originality of the research

For the first time, investigations of the SPP and IPP characteristics of ZnO thin film on 6H-SiC substrate and ZnO/GaN heterostructure on 6H-SiC substrate are reported. Owing to a lack of comparative experimental and theoretical studies of the SPP mode in bulk ZnO crystal in the literature, the SPP characteristics of bulk ZnO crystal are re-examined. Apart from that, a new formulation of the SP dispersion relation for wurtzite based multilayer system is developed. The formulation is derived through a different technique as compared to the reported one.

1.4 Organization of the dissertation

After a brief introduction in this chapter, the fundamental concepts of the phonon polariton, SPP and IPP phenomena, history of research on the SPP and IPP modes, and previous studies of the SPP and IPP modes in ZnO-based semiconductor structures are reviewed briefly in chapter 2. Chapter 3 presents the theoretical models used for the simulation of the SP dispersion curves, the polarized IR reflectance and the ATR spectra. Chapter 4 describes the details of the samples and the experimental techniques employed in this study. The experimental setup and operating principles for each experiment will be discussed in brief. Chapters 5 and 6 illustrate the main results of the research. Preliminary theoretical studies of the SPP and IPP modes in bulk ZnO crystal, ZnO thin film on 6H-SiC substrate, and ZnO/GaN heterostructure on 6H-SiC substrate are given in chapter 5, followed by their experimental verifications in chapter 6. Finally, chapter 7 summarizes the important results of the dissertation and suggests possible directions for future research.

CHAPTER 2

LITERATURE REVIEW

2.1 Introduction

This chapter discusses some important contributions to the field of study. First, the fundamentals of phonon polariton, SPP and IPP will be reviewed briefly. Next, the history of research on the SPP and IPP modes, followed by an overview of previous studies on the SPP and IPP modes in ZnO-based semiconductor structures will be given to highlight the importance aspects relevant to this work.

2.2 Introduction to phonon polariton

The atoms of a crystal are bound to their equilibrium positions by the forces that hold the crystal together. When the atoms are displaced from their original positions, they experience restoring forces and vibrate at certain frequencies called phonon modes (Cardona and Yu, 2005; Fox, 2010).

It is well known that when EM wave propagate into a polar dielectric medium, the photon can couple with an elementary particle or excitation (phonon, plasmon, exciton, etc.) to form a mixed mode called polariton (Mills and Burstein, 1974; Agranovich and Mills, 1982; Cottam and Tilley, 1989; Albuquerque and Cottam, 2004). In the case of the IR photon couple with an optical phonon, the resulting mixed mode is known as phonon polariton. Similarly, the photon-plasmon and the photon-exciton interactions give rise to the plasmon polariton and exciton polariton, respectively.

Fig. 2.1 shows the dispersion relation of the bulk phonon polariton (BPP) mode in a bulk cubic crystal. Due to the EM wave is transverse mode and can only apply driving forces to the transverse vibrations of the crystal, therefore, the photon can only couple with the transverse optical (TO) phonon but not with the longitudinal optical (LO) phonon, as demonstrated experimentally by Henry and Hopfield (1965).
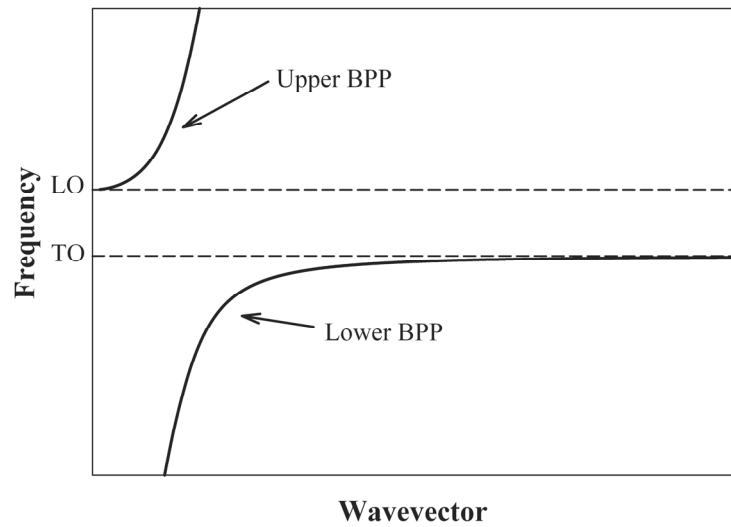
Fig. 2.1: Bulk phonon polariton (BPP) dispersion curve for a bulk cubic crystal.

In addition, the photon-phonon coupling can only happen if the atoms in the crystal are charged. This means that the formation of phonon polariton is limited to the crystal that contains ionic character, i.e., a crystal consists of alternating sequence of positive and negative ions that are held together by Coulomb forces. The bond with ionic character is called polar bond, which causes the phonon to interact directly with the incident IR photon. The phonon that can interact directly with the IR photon is known as IR active mode (Mills and Burstein, 1974; Boardman, 1982; Stroscio and Dutta, 2001; Cardona and Yu, 2005; Fox, 2010).

2.3 Surface phonon polariton (SPP) and interface phonon polariton (IPP) phenomena

The lattice vibrations of atoms near the surface of a crystal have different frequencies from those of bulk vibrations because on the vacuum side of the surface, the restoring forces are missing. The quanta of surface vibrations are known as surface phonons (Lüth, 2010).

SPP phenomenon arises when the incident photon with transverse magnetic (TM) mode couple to the surface phonon localized near the surface of a polar crystal. The SPP mode travels along a direction perpendicular to the surface normal, and its amplitude attenuates exponentially from surface to bulk (Mills and Burstein, 1974; Agranovich and Mills, 1982; Boardman, 1982; Wallis and Stegeman, 1986; Cottam and Tilley, 1989; Albuquerque and Cottam, 2004). One of the unique characteristics of the SPP is that it can propagate through the forbidden band of the BPP, where the dielectric function of the crystal is negative (i.e., interval between the TO and LO phonon frequencies) and results in surface enhanced IR absorption (Kim and Cheng, 2010b).

Note that a material having a negative dielectric function is known as a surface active medium, which supports the surface mode when it attaches with a surface inactive medium having a positive dielectric function (Burstein et al., 1974; Holm and Palik, 1978). While, the frequency region for the propagation of SPP mode is known as the surface-mode window (Cottam and Tilley, 1989). For clarity, the schematic diagram of the dispersion relation of the SPP and BPP modes in a bulk cubic crystal together with a vacuum light line is shown in Fig. 2.2 and indicated by solid line, dotted line, and dash-dot line, respectively.
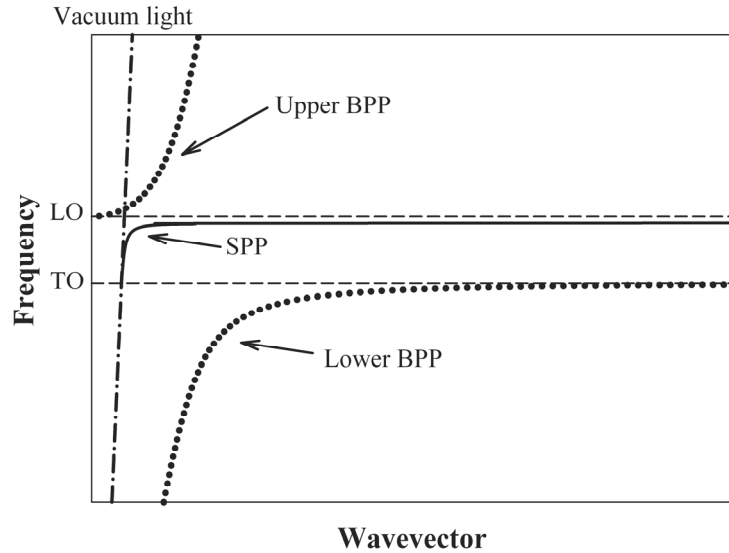
Fig. 2.2: SPP (solid line) and BPP (dotted line) dispersion curves for a bulk cubic crystal.

In a multilayer structure with polar media, polarization charges exist at both the surface and interfaces. Consequently, in addition to the SPP mode, there are interface phonon polariton (IPP) modes that propagate along the interfaces of the system. The SPP and IPP modes in a multilayer structure exhibit more complicated characteristics than a simple semi-infinite/semi-infinite structure (Marschall and Fischer, 1972; Mills and Maradudin, 1973; Halevi, 1978; Holm and Palik, 1978). For example, in a vacuum/GaP two layer structure, the SPP mode of GaP just depends on its dielectric function (Marschall and Fischer, 1972). On the contrary, in a vacuum/GaAs/sapphire three-layer structure, the SPP mode of GaAs and the IPP mode of GaAs/sapphire were shown to vary greatly depending on the GaAs layer thickness as well as both the dielectric functions of GaAs layer and sapphire substrate (Mills and Maradudin, 1973).

In view of the application potential of the SPP and IPP in various fields, extensive research has been carried out to explore the SPP and IPP characteristics of

9

various materials. Nevertheless, the research of the SPP and IPP in many practical materials is still found to be insufficient, particularly the wurtzite semiconductor heterostructure, as discussed later in section 2.4.

2.4 History of research on the SPP and IPP modes

The SPP and IPP phenomena have been reported since a few decades ago. Early studies on the SPP and IPP were concentrated on the cubic structure materials. For instances, Fischer et al. (1974) studied the SPP modes in $SrTiO_3$ and $KTaO_3$ crystals. Bryksin et al. (1972; 1974) studied the SPP modes in CaF_2, CdF_2, and several alkali halide crystals. Watanabe et al. (1983; 1984) investigated the SPP mode in ZnTe slab. Nakayama et al. (1988; 1990) investigated the SPP and IPP modes in GaAs/AlAs heterostructure on GaAs substrate.

In recent years, the studies of the SPP and IPP modes are focused on wurtzite structure materials. Particular attention has been paid to the III-nitride semiconductors and their alloy systems. For instances, Kuroda et al. (2005) studied the SPP and IPP modes in GaN thin film on sapphire substrate. Zhang and Shi (2009) studied the SPP and IPP modes in $Al_xGa_{1-x}N$ thin film. Valcheva et al. (2009; 2010) investigated the SPP and IPP modes in InN/AlN heterostructure on sapphire substrate. Ng et al. (2007a; c; 2008a; b; 2009a; b; 2009c; 2010a; 2010b) carried out the studies of the SPP and IPP modes in several III-nitride-based binary, ternary, and quaternary compounds.

It is worth to highlight here that owing to the effects of uniaxial anisotropy, the SPP and IPP modes in wurtzite structure materials revealed several distinct behaviors as compared to those of cubic structure materials. For example, the virtual SPP mode may exists in wurtzite crystal, however, this mode is absent in cubic

crystal (Perry et al., 1973; Chu and Bates, 1986; El-Gohary et al., 1989; Costa Filho et al., 1996). The reason is that there is only one set of dielectric tensor components that describes the phonon properties of cubic crystal whereas, two sets of dielectric tensor components are required to describe the phonon properties of wurtzite crystal (Barker and Ilegems, 1973; Vasiljev, 2002; Kroon, 2007; Kuroda and Tabata, 2010; Lee et al., 2011c).

In spite of numerous investigations on the SPP and IPP modes in a variety of materials, there are only a few reports on the SPP and IPP modes in wurtzite semiconductor heterostructures with more than three or four interfaces (Valcheva et al., 2009; Ng et al., 2010a; 2010b). In semiconductor device fabrication, there are layers that are intentionally grown or deposited. Meanwhile, accumulation layers and oxide layers may exist at the surface and interfaces. In all these cases, the lattice dynamics as well as the other properties related to the surface and interface regions might be altered (Stroscio and Dutta, 2001; Lüth, 2010).

To obtain accurate information about the SPP and IPP modes, one must consider a multilayer or a multi-interface configuration in the numerical analysis of these modes. Consequently, a systematic study of the SPP and IPP modes in wurtzite based multilayer system is essential, which is one subject of interest in this dissertation.

2.5 Overview of studies on the SPP and IPP modes in wurtzite ZnO-based semiconductor structures

The SPP and IPP characteristics of ZnO-based semiconductor structures are remain unclear at present. Although the SPP and IPP phenomena have been

discovered a few decades ago, the studies of the SPP and IPP modes in wurtzite ZnO-based semiconductor structures are rarely reported.

Previously, Dovbeshko et al. (1984) have reported experimental investigations on the SPP and IPP modes in bulk ZnO crystal and ZnO thin film on fused quartz substrate. Inadequately, there are no relevant theoretical results provided for comparison. In 2004, Dovbeshko et al. have reexamined the SPP and IPP modes in ZnO thin film on fused quartz substrate and analyzed the observation with a theoretical treatment. However, their calculations did not consider the effects of anisotropy in the ZnO thin film.

The study of the SPP and IPP modes in ZnO thin film on sapphire substrate have been reported by Beletskii et al. (1994). In this study, the effects of anisotropy in both the ZnO thin film and sapphire substrate have been taken into account in the calculations. The results indicated that the conditions and the ranges of existence of the SPP and IPP modes in wurtzite structure media are strongly dependent upon their anisotropic parameters.

It should be pointed out that in the above studies of the SPP and IPP modes in the ZnO thin film, the reststrahlen bands of the substrates (fused quartz and sapphire) overlapped with that of the ZnO thin film. Consequently, the behavior of the SPP and IPP modes in ZnO heterostructures is still not clearly understood. Moreover, in the above studies, the parameters used in the calculations were taken from literatures instead of obtained directly from the characterization of real samples, which may reduce the accuracy of the results. For all the reasons mentioned above, in-depth experimental and theoretical investigations are highly demanded to clarify the SPP and IPP characteristics of wurtzite ZnO-based semiconductor structures.

2.6 Summary

The basic concepts of the phonon polariton, SPP and IPP have been reviewed in brief. Some of the previous studies and the current interest in the research field of the SPP and IPP were also discussed. Throughout this chapter, a clear picture of the research status of the SPP and IPP modes in wurtzite ZnO-based semiconductor structures has been illustrated.

CHAPTER 3

THEORETICAL MODEL

3.1 Introduction

In this chapter, the theoretical models used for the simulation of the SP dispersion curves, the polarized IR reflectance and the ATR spectra will be introduced. The step-by-step algebraic derivations of each equation will be described in detail. To realize all these simulations, the initial approach is to determine the dielectric tensor components of the studied material. Therefore, a description of the dielectric function model used in this study will be given first. The final section of this chapter discusses the relationship between the SP dispersion relation and the p-polarized IR reflectivity.

3.2 Dielectric function of the wurtzite crystal

Dielectric properties are greatly dependent on the crystal symmetry. For wurtzite crystal with optical axis (c_{axis}) along the growth direction ($c_{axis} \parallel z$) and perpendicular to the propagation direction ($c_{axis} \perp x$), two sets of dielectric tensor components are required to describe its dielectric properties; one set to $\varepsilon_{xx} = \varepsilon_{yy} = \varepsilon_{\perp}$ and another set to $\varepsilon_{zz} = \varepsilon_{\parallel}$. Taking into account both the contributions of lattice vibrations (phonon) and free carriers (plasmon), the dielectric function model is given by (Gervais and Piriou, 1974; Kroon, 2007):

$$\varepsilon_j(\omega) = \varepsilon_{\infty j}\left(\frac{\omega_{LOj}^2 - \omega^2 - i\omega\gamma_{LOj}}{\omega_{TOj}^2 - \omega^2 - i\omega\gamma_{TOj}} - \frac{\omega_{pj}^2}{\omega^2 + i\omega\gamma_{pj}}\right),$$ (3.1)

where ε_{∞} is the high-frequency dielectric constant, ω is the angular frequency, ω_{LO} and ω_{TO} are the LO and TO phonon frequencies, respectively. γ_{LO} and γ_{TO} are the LO and TO phonon damping constants, respectively. ω_p is the plasma frequency, and γ_p is the plasma damping constant. The subscript j represents the parallel ($\parallel$) and perpendicular ($\perp$) vibrational modes with respect to the c_{axis}.

3.3 Surface polariton (SP) dispersion relation

Generally, the SP dispersion relation can be derived through solving Maxwell's EM equations directly using the boundary conditions at the interfaces. Emphasis is paid to the TM surface wave that propagates in the x direction with electric vectors in the xz plane. Following the approach introduced by (Mills and Maradudin, 1973), Maxwell's EM equations are given by:

$$ik_x \frac{dE_z(z)}{dz} - \frac{d^2E_x(z)}{dz^2} = \left(\frac{\omega}{c}\right)^2 D_x(z),$$ (3.2)

$$ik_x \frac{dE_x(z)}{dz} + k_x^2 E_z(z) = \left(\frac{\omega}{c}\right)^2 D_z(z),$$ (3.3)

$$H_y(z) = \frac{c}{i\omega}\left(\frac{dE_x(z)}{dz} - ik_x E_z(z)\right).$$ (3.4)

Here, $D_x(z)$ and $D_z(z)$ are the electric displacement field components along the x and z directions. Their relations are given by $D_x(z) = \varepsilon_\perp E_x(z)$ and $D_z(z) = \varepsilon_\parallel E_z(z)$,

respectively. $E_x(z)$ and $E_z(z)$ are the electric field components along the x and z direction, respectively. $H_y(z)$ is the auxiliary magnetic field component along the y direction. k_x is the wavevector of the SP along the x direction and c is the velocity of light in a vacuum $(3 \times 10^8 \text{ ms}^{-1})$.

3.3.1 Two-layer system

Consider a two-layer system with the geometry and the coordinate system as shown in Fig. 3.1. In Fig. 3.1, the layer in the system is denoted by l, i.e., $l = 1$ for the medium of incidence and $l = 2$ for the bulk crystal. Each layer is assumed to be anisotropic and having an anisotropic dielectric function $\varepsilon_{l,\perp(\parallel)}$.
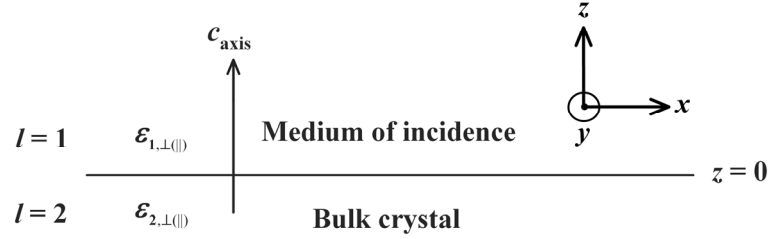
Fig. 3.1: Schematic diagram of a wurtzite based two-layer system together with the geometry and the coordinate system used.

The standard solutions of Eqs. (3.2) - (3.4) for the two semi-infinite regions ($z > 0$ and $z < 0$) described in Fig. 3.1 can be written as:

$$E_x(z) = A \exp(-\alpha_0 z)$$

$$= \frac{-i\alpha_0}{k_x}\left(\frac{\varepsilon_{1,\parallel}}{\varepsilon_{1,\perp}}\right)E_z(z) = \frac{i\alpha_0}{\varepsilon_{1,\perp}}\left(\frac{c}{\omega}\right)H_y(z) , \qquad (3.5)$$

16

for $z > 0$, and

$$E_x(z) = B \exp(\alpha_1 z)$$

$$= \frac{i\alpha_1}{k_x}\left(\frac{\varepsilon_{2,\parallel}}{\varepsilon_{2,\perp}}\right)E_z(z) = -\frac{i\alpha_1}{\varepsilon_{2,\perp}}\left(\frac{c}{\omega}\right)H_y(z) , \qquad (3.6)$$

for $z < 0$.

The symbols α_0 and α_1 are the field decay constants along the normal of the interface, which can be determined from the relation (Mills and Maradudin, 1973):

$$\alpha_{(l-1)} = \sqrt{\frac{\varepsilon_{l,\perp}}{\varepsilon_{l,\parallel}}k_x^2 - \varepsilon_{l,\perp}\left(\frac{\omega}{c}\right)^2} . \qquad (3.7)$$

Using the continuity of D_z (or H_y) and E_x at the interface ($z = 0$), a set of homogeneous equations for the coefficients A and B in Eqs. (3.5) and (3.6), which admit a non trivial solution only if

$$\frac{\alpha_0}{\varepsilon_{1,\perp}} + \frac{\alpha_1}{\varepsilon_{2,\perp}} = 0 . \qquad (3.8)$$

Equation (3.8) is the implicit SP dispersion relation for a two-layer system (Mills and Burstein, 1974). By substituting Eq. (3.7) into Eq. (3.8) and through simple algebraic arrangement, an explicit form for Eq. (3.8) can be obtained as:

$$k_x = \left(\frac{\omega}{c}\right)\sqrt{\frac{\varepsilon_{1,\parallel}(\varepsilon_{2,\parallel}\varepsilon_{2,\perp} - \varepsilon_{2,\parallel}\varepsilon_{1,\perp})}{\varepsilon_{2,\parallel}\varepsilon_{2,\perp} - \varepsilon_{1,\parallel}\varepsilon_{1,\perp}}} . \qquad (3.9)$$

3.3.2 Three-layer system

The schematic diagram of a three-layer system together with the geometry and the coordinate system used is described in Fig. 3.2. In comparison to section 3.3.1, there is a thin film with finite thickness d located between the medium of incidence and substrate (bulk). Hence, two interfaces involve in the derivation of the SP dispersion relation.

Fig. 3.2: Schematic diagram of a wurtzite based three-layer system together with the geometry and the coordinate system used.

The standard solutions of Eqs. (3.2) - (3.4) for the three regions ($z > 0$, $-d < z < 0$, and $z < -d$) described in Fig. 3.2 are given by Eq. (3.5) for $z > 0$,

$$E_x(z) = B_1 \exp(\alpha_1 z) + B_2 \exp(-\alpha_1 z)$$

$$= \frac{i\alpha_1}{k_x}\left(\frac{\varepsilon_{2,\|}}{\varepsilon_{2,\perp}}\right) E_z(z) = -\frac{i\alpha_1}{\varepsilon_{2,\perp}}\left(\frac{c}{\omega}\right) H_y(z) \ , \tag{3.10}$$

for $-d < z < 0$, and

$$E_x(z) = C \exp(\alpha_2 z)$$

$$= \frac{i\alpha_2}{k_x}\left(\frac{\varepsilon_{3,\|}}{\varepsilon_{3,\perp}}\right)E_z(z) = -\frac{i\alpha_2}{\varepsilon_{3,\perp}}\left(\frac{c}{\omega}\right)H_y(z), \qquad (3.11)$$

for $z < -d$.

Using the continuity of D_z (or H_y) and E_x at the two interfaces ($z = 0$ and $z = -d$), a set of homogeneous equations for the coefficients A, B_1, B_2, and C in Eqs. (3.5), (3.10), and (3.11), which admit a non trivial solution only if

$$(\alpha_1\varepsilon_{1,\perp} + \alpha_0\varepsilon_{2,\perp})(\alpha_1\varepsilon_{3,\perp} + \alpha_2\varepsilon_{2,\perp}) - (\alpha_1\varepsilon_{1,\perp} - \alpha_0\varepsilon_{2,\perp})(\alpha_1\varepsilon_{3,\perp} - \alpha_2\varepsilon_{2,\perp})\exp(-2\alpha_1 d) = 0.$$
$$(3.12)$$

Equation (3.12) is the SP dispersion relation for a three-layer system (Boardman, 1982; Beletskii et al., 1994). However, unlike two-layer system, an explicit form for Eq. (3.12) is not available because Eq. (3.12) is a transcendental equation, which cannot be solved algebraically. However, approximate solutions of Eq. (3.12) can be determined by the standard numerical root finding procedures. The methods for solving this problem can be found from many textbooks (Press, 2007; Salleh et al., 2007; Hauser, 2009; Dos Passos, 2010).

3.3.3 Multilayer system

Consider a multilayer system composed of N wurtzite layers as shown in Fig. 3.3. There are N-2 thin films with finite thicknesses (d_1, d_2, ..., d_{N-2}) located between the medium of incidence and the substrate. Therefore, the derivation of the SP dispersion relation involves N - 1 interfaces, where the interface between layer l and layer $l + 1$ is denoted by m ($m = 1, 2, ..., N$ - 1).
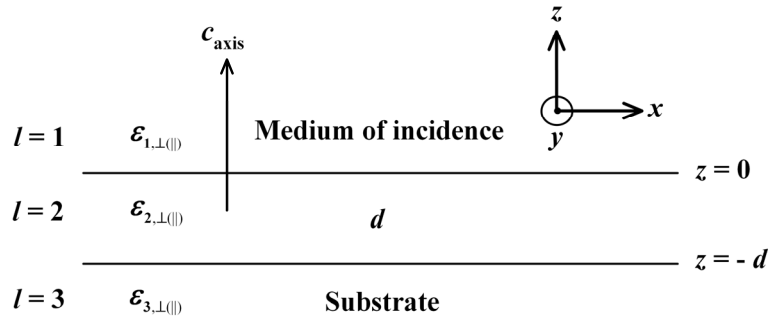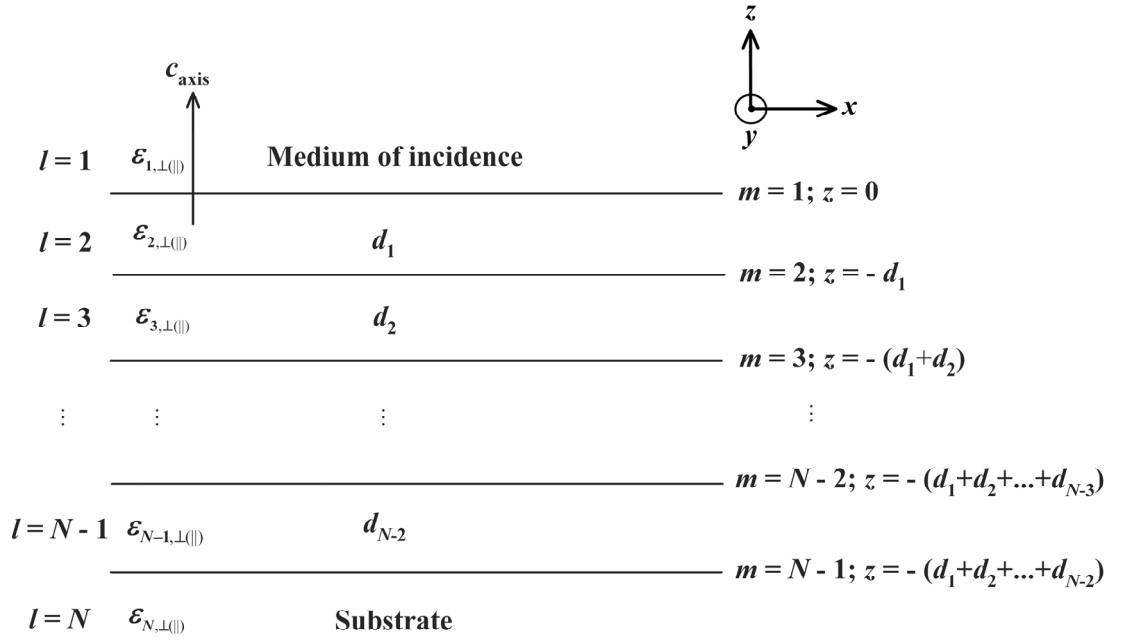
Fig. 3.3: Schematic diagram of a wurtzite based multilayer system together with the geometry and the coordinate system used (Lee et al., 2011a).

Although the problem solving in this case involves many interfaces, however, the equations of electric field components for $l = 2$ until $l = N - 1$ (thin film region) have similar forms. Consequently, the standard solutions of Eqs. (3.2) - (3.4) for multilayer system are just similar to the case of three-layer system, i.e., Eq. (3.5) for $z > 0$,

$$E_x(z) = B_{l,1} \exp(\alpha_{l-1}z) + B_{l,2} \exp(-\alpha_{l-1}z)$$

$$= \frac{i\alpha_{l-1}}{k_x}\left(\frac{\varepsilon_{l,\|}}{\varepsilon_{l,\perp}}\right) E_{l,z}(z) = -\frac{i\alpha_{l-1}}{\varepsilon_{l,\perp}}\left(\frac{c}{\omega}\right) H_y(z), \tag{3.13}$$

for $-\sum_{j=1}^{N-2} d_j < z < 0$ $(l = 2, 3, \ldots, N\text{-}1)$, and

$$E_{N,x}(z) = C \exp(\alpha_{N-1}z)$$

20

$$= \frac{i\alpha_{N-1}}{k_x}\left(\frac{\varepsilon_{N,\parallel}}{\varepsilon_{N,\perp}}\right)E_{N,z}(z) = -\frac{i\alpha_{N-1}}{\varepsilon_{N,\perp}}\left(\frac{c}{\omega}\right)H_y(z)\,, \tag{3.14}$$

for $z < -\sum_{j=1}^{N-2}d_j$.

By applying the continuity of D_z (or H_y) and E_x at the m interfaces ($z = 0$, $-d_1$, $-(d_1 + d_2)$, …, $-\sum_{j=1}^{N-2}d_j$) for $N = 3, 4, 5$, etc., the SP dispersion relations for $N = 3, 4, 5$, etc. can be subsequently derived. However, it is found that the expressions of the SP dispersion relation for $N > 5$ are sophisticated. For this reason, some algebraic manipulations and sorting operations are carried out to understand the pattern of the SP dispersion relation as N increases. Ultimately, a general formulation of the SP dispersion relation for wurtzite based multilayer system is derived and is implicitly written as (Lee et al., 2011a):

$$\frac{F_{N,+}}{u_{N-1}} + \frac{F_{N,-}}{v_{N-1}} = 0\,. \tag{3.15}$$

Here, u_{N-1} and v_{N-1} are determined using

$$u_m = \alpha_{m-1}\varepsilon_{m+1,\perp}\,, \tag{3.16}$$

$$v_m = \alpha_m\varepsilon_{m,\perp}\,. \tag{3.17}$$

The expression of $F_{N,\pm}$ is very complicated. Thus, several symbols are adopted as the intermediate functions for simplification. The first symbol introduced is f_r, which is described as a function of binary value (1 or 0), as follow:

21

$$f_r(1) = \exp(\alpha_r d_r), \tag{3.18}$$

$$f_r(0) = \exp(-\alpha_r d_r), \tag{3.19}$$

where $r = 1, 2, \ldots, N\text{-}3, N\text{-}2$. A reverse function of r is given by

$$\mathrm{rev}(r) = N - r - 1. \tag{3.20}$$

The multiplication of $f_{\mathrm{rev}(r)}$ gives function M_n:

$$M_n = \prod_{r=1}^{N-2} \left[f_{\mathrm{rev}(r)}(\beta_N(n,r)) \right], \tag{3.21}$$

where $n = 1, 2, \ldots, n_{\max}$ and $n_{\max} = 2^{N-2}$. $\beta_N(n,r)$ refers to the matrix element of β_N.

The β_N is given by:

$$\beta_N = \begin{bmatrix} \beta_N(1,1) & \beta_N(1,2) & \cdots & \beta_N(1,N-2) \\ \beta_N(2,1) & \beta_N(2,2) & \cdots & \beta_N(2,N-2) \\ \vdots & \vdots & \cdots & \vdots \\ \beta_N(n_{\max},1) & \beta_N(n_{\max},2) & \cdots & \beta_N(n_{\max},N-2) \end{bmatrix}. \tag{3.22}$$

The matrix row of Eq. (3.22) is a binary function that is used to convert ordinary number n - 1 to binary values and is given by:

$$\beta_N(n:,) = \begin{bmatrix} \beta_N(n,1) & \beta_N(n,2) & \cdots & \beta_N(n,N-2) \end{bmatrix} = \mathrm{binary}(n-1). \tag{3.23}$$

Next, $Q_{i,\pm}$ is defined as:

$$Q_{i,\pm} = \sum_{j=i_{\max}+1}^{n_{\max}} \left[g_N(i, j - i_{\max}) \times M_j \right] \pm \sum_{j=1}^{i_{\max}} \left[g_N(i, j) \times M_j \right], \qquad (3.24)$$

where $i = 1, 2, \ldots, i_{\max}$ and $i_{\max} = 2^{N-2}/2$. $g_N(i, j)$ refers to the positive (+) or negative (-) sign, which is the matrix element in:

$$g_N = \begin{pmatrix} -g_{N-1} & g_{N-1} \\ g_{N-1} & g_{N-1} \end{pmatrix}$$

$$= \begin{bmatrix} g_N(1,1) & g_N(1,2) & \cdots & g_N(1, i_{\max}) \\ g_N(2,1) & g_N(2,2) & \cdots & g_N(2, i_{\max}) \\ \vdots & \vdots & \cdots & \vdots \\ g_N(i_{\max},1) & g_N(i_{\max},2) & \cdots & g_N(i_{\max}, i_{\max}) \end{bmatrix}. \qquad (3.25)$$

Equation (3.25) is a recursive function, it can be initialized by $g_3 = (+)$. Other recursive functions involved in the calculation of $F_{N,\pm}$ are given by:

$$U_N = u_{N-2} \begin{pmatrix} V_{N-1} \\ U_{N-1} \end{pmatrix} = \begin{bmatrix} U_N(1) \\ U_N(2) \\ \vdots \\ U_N(i_{\max}) \end{bmatrix}, \qquad (3.26)$$

$$V_N = v_{N-2} \begin{pmatrix} U_{N-1} \\ V_{N-1} \end{pmatrix} = \begin{bmatrix} V_N(1) \\ V_N(2) \\ \vdots \\ V_N(i_{\max}) \end{bmatrix}. \qquad (3.27)$$

Equations (3.26) and (3.27) can be initialized by $U_3 = (u_1)$ and $V_3 = (v_1)$, respectively. Eventually, $F_{N,\pm}$ can be calculated using:

$$F_{N,\pm} = \sum_{j=1}^{i_{max}} \left[Q_{j,\pm} V_N(j) + Q_{j,\mp} U_N(j) \right]. \tag{3.28}$$

Generally, Eq. (3.15) is working well for $N > 2$. However, when $N = 2$, both $F_{2,+}$ and $F_{2,-}$ are undefined because Eq. (3.28) is only applicable for $N \geq 3$. This is because $F_{N,\pm}$ is related to the presence of the thin film layers between the medium of incidence and the substrate. For instance, the intermediate functions that involved in the calculation of $F_{N,\pm}$ [Eqs. (3.18) - (3.27)] require the finite thickness of each thin film [Eqs. (3.16) - (3.18)] and the minimum N as 3 [Eqs. (3.19) - (3.26)]. However, if let $F_{2,+} = F_{2,-} = F$, Eq. (3.15) can be expressed as:

$$F(\frac{1}{u_1} + \frac{1}{v_1}) = 0. \tag{3.29}$$

Although F is an undefined factor for $N = 2$, however, Eq. (3.29) is still valid due to the factor of $\frac{1}{u_1} + \frac{1}{v_1}$ is physically true for $N = 2$. According to the definition of u and v [Eqs. (3.16) and (3.17)], these two parameters depend on the interface m. For a two-layer system ($N = 2$), an interface still exists, therefore,

$$\frac{1}{u_1} + \frac{1}{v_1} = 0. \tag{3.30}$$

By substituting the expressions of u_1 and v_1 into Eq. (3.30) and through simple rearrangement, Eqs. (3.8) and (3.9), which are the well known SP dispersion relations for a two-layer system can be yielded.

It is worth to mention here that the above formulation can also be used for cubic based multilayer system or mix cubic/wurtzite based multilayer system in